SIMULATION OF THE WATER CYCLE ON MARS IN THE CCSR/NIES/FRCGC MGCM. Takeshi Kuroda[1,2], Paul Hartogh[2], Daisuke Sakai[3] and Masaaki Takahashi[3], [1]Institute of Space and Astronautical Science, Japan Aerospace Exploration Agency, Japan *(kuroda@isas.jaxa.jp)*, [2]Max-Planck-Institute for Solar System Research, Katlenburg-Lindau, Germany, [3]Center for Climate System Research, University of Tokyo, Japan.

Introduction: There is already a lot of data for the column density distributions of water vapor and water ice from Mars Global Surveyor, Mars Express and other missions [1,2]. In addition, the ground-based microwave telescopes have observed the abundance of H_2O and HDO in Martian atmosphere [3,4], and detected the hygropause (cut-off height of water vapor) on Martian low- and mid-latitude, which varies from <10 km (around aphelion, northern summer) and >25 km (around perihelion, northern winter) depending on the season [5]. The seasonal change of hygropause and the ratio of HDO/H_2O will also be observed by the upcoming Herschel space telescope (launch in the end of 2008).

3-dimensional simulation of the atmospheric water cycle is an important step in understanding the Martian atmosphere, for the theoretical interpretation of the observational data. The investigation of the vertical distributions of water vapor/ice is especially important, because the water can be transported from summer to winter hemisphere only when the hygropause is high enough, as well as the water ice should significantly determine the temperature distributions. The investigation of the HDO/H_2O ratio is the key to understand the climate evolutions of Mars.

Here we introduce a water cycle in our Martian general circulation model, CCSR/NIES/FRCGC MGCM (updated version of the CCSR/NIES MGCM [6]). We show first results obtained with a simple water cycle scheme.

Description of the MGCM: The MGCM is based on the spectral solver for the three-dimensional primitive equations. The horizontal resolution is set at about $5.6^\circ \times 5.6^\circ$ (~333 km at equator), the vertical grid consists of 30 σ-levels with the top of the model at about 80 km. Realistic topography, albedo and thermal inertia data for the Mars surface, and CO_2 condensation/sublimation processes are included. Radiative effects of CO_2 gas (considering only LTE) and dust, in solar and infrared wavelengths, are taken into account. The amount of atmospheric dust varies with season and latitude, imitating the observational data in MY24 (MY24 dust scenario, Figure 1), except in the global dust storm case.

Water cycle scheme. The schematic features of the water cycle are seen in Figure 2. The condensation of supersaturated water vapor is calculated using a large scale condensation scheme. The condensed water ice falls by the gravitational sedimentation (the particle radius is set to 2 μm), and is deposited on surface. With surface water ice, the surface albedo changes to 0.3-0.4. Sublimation of the surface water ice is introduced by the turbulent flux.

The microphysical processes, absorption by regolith, and radiative effects of water vapor/ice are not included.

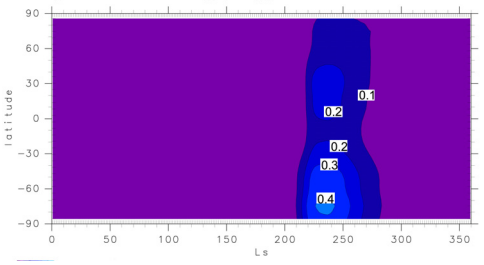

Figure 1: Time-latitude cross-sections of the zonal-mean dust optical depth in infrared wavelengths (9-10 μm) at surface in the MY24 dust scenario.

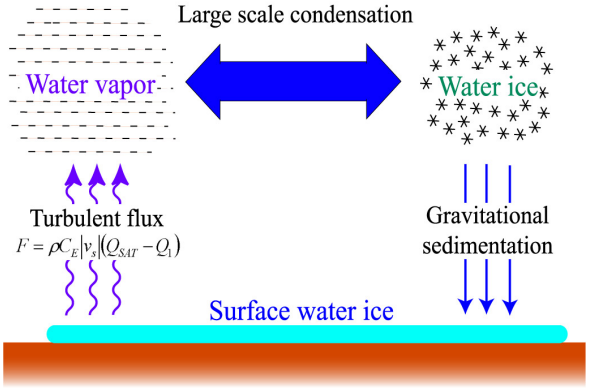

Figure 2: Schematic features of the water cycle scheme.

Model results: The calculations start from northern spring equinox, with isothermal conditions (200 K), constant surface pressure (7.6 mb), water vapor distributions linearly decreasing with latitude (150 ppm at north pole to 0 ppm at south pole), no CO_2 and no water ice. We show the fourth model year results.

In the low-dust case (MY24 dust scenario). Figure 3 shows the comparison of atmospheric temperature between the model (with MY24 dust scenario) and the corresponding MGS-TES observations. The lower temperature in the equatorial middle (0.1-1 mb height) atmosphere of the model is possibly due to the lack of the radiative effects of water ice [7]. Except that, the model results are mostly consistent with the observations.

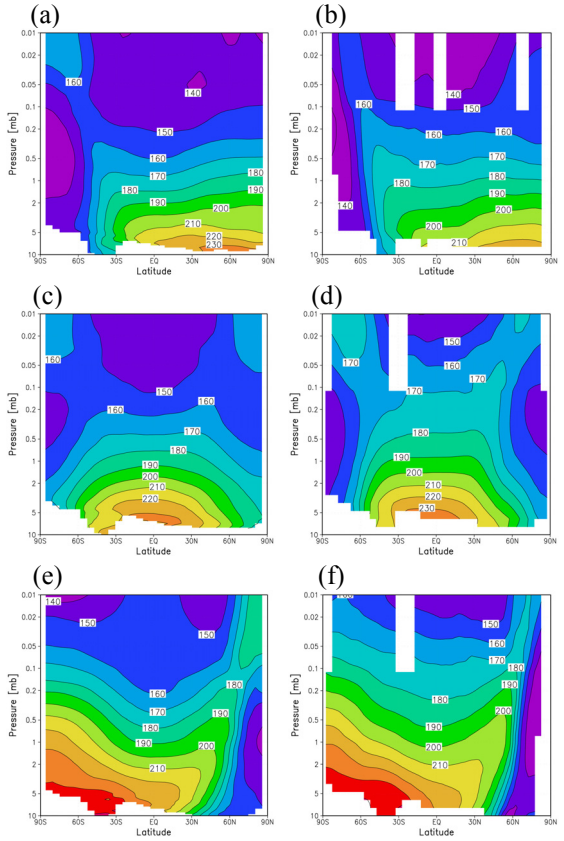

Figure 3: Zonal-mean day-mean temperature [K] in L_s=90˚, (a) for the MGCM results and (b) corresponding MGS-TES nadir+limb observational data. (c) and (d) are same as (a) and (b), respectively, except for L_s=180˚. (e) and (f) are the same as (a) and (b), respectively, except for L_s=270˚.

Figure 4 shows the seasonal change of the zonal-mean water ice column density in comparison between model and observation. In the present simulation, the equatorial cloud belt in northern summer is much thinner than the observation.

Figure 5 shows height-latitude cross-sections of the simulated water ice distributions. The height of the equatorial cloud indicates the hygropause, as discussed below.

Figure 6 shows the same as Figure 4, except for water vapor. In the present simulation, the amount of atmospheric water vapor in southern summer is much less than in the observations. In northern summer, the results are mostly consistent between model and observations.

Figure 7 shows height-latitude cross-sections of the simulated water vapor distributions. Water vapor can exist only below the water ice clouds. If we define the hygropause as the highest point with the water vapor of ~5 ppm, it is 0.5-1.0 mb (15-20 km height) in L_s=90° and 180°. In L_s=270°, the hygropause reaches to ~0.04 mb (~48km height) above the south pole, while ~0.2 mb (~30 km height) above the equator.

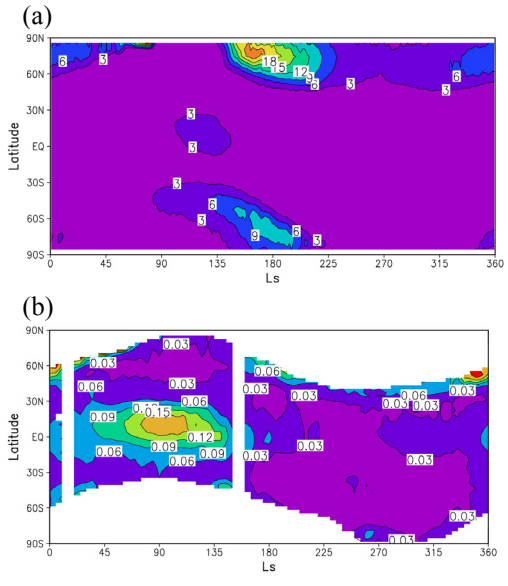

Figure 4: Time-latitude cross-sections of the zonal-mean water ice column density: (a) MGCM results [pr.μm] and (b) MGS-TES observational data [optical depth at 825 cm^{-1}].

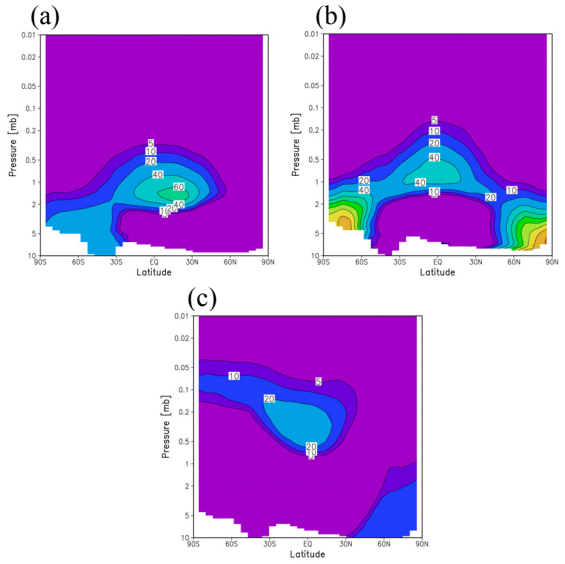

Figure 5: Zonal-mean mass mixing ratio of water ice [ppm] in (a) L_s=90˚, (b) L_s=180˚ and (c) L_s=270˚ for the MGCM results.

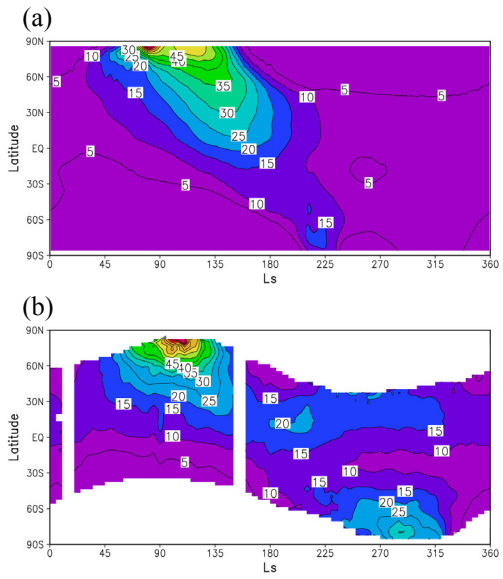

Figure 6: Time-latitude cross-sections of the zonal-mean water vapor column density [pr.μm]: (a) MGCM results and (b) MGS-TES observational data.

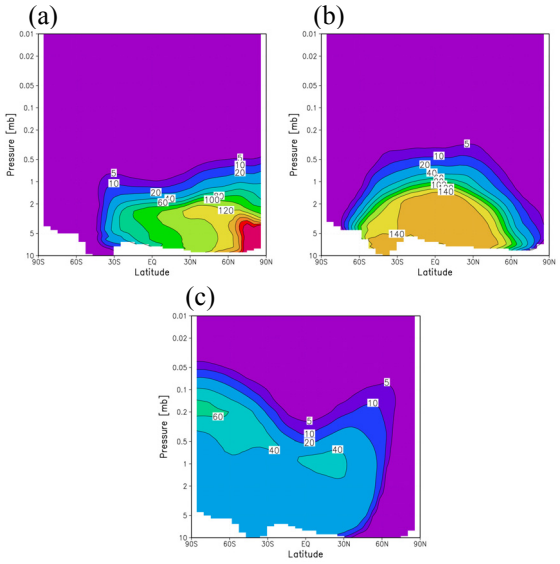

Figure 7: Zonal-mean mass mixing ratio of water vapor [ppm] in (a) L_s=90˚, (b) L_s=180˚ and (c) L_s=270˚ for the MGCM results.

In the global dust storm case. Figures 8 shows the simulated temperature and water distributions in the global dust storm conditions for northern winter (L_s=290°), with global-mean visible dust opacity of 4.2, as observed in 1977. In this case the hygropause reaches to the top of the model, and water ice of >5 ppm exists only above ~0.02 mb (~56km height) at the equator.

In the limb-haze observation by the Viking Orbiter, the water ice exists at 50-90 km height in this condition [8], which means the hygropause is higher than 50 km. The MGCM results have a consistency with this.

Summary: Though there are some inconsistencies with the MGS-TES observations (e.g. thin equatorial cloud belt in northern summer, disappearance of water vapor in northern winter), the MGCM well reproduces the change of hygropause in different season and dust opacity detected by ground-based microwave telescopes and limb-haze observations from a spacecraft. This model will help to investigate the meridional transport of water on Mars, combined with the upcoming observations by Herschel.

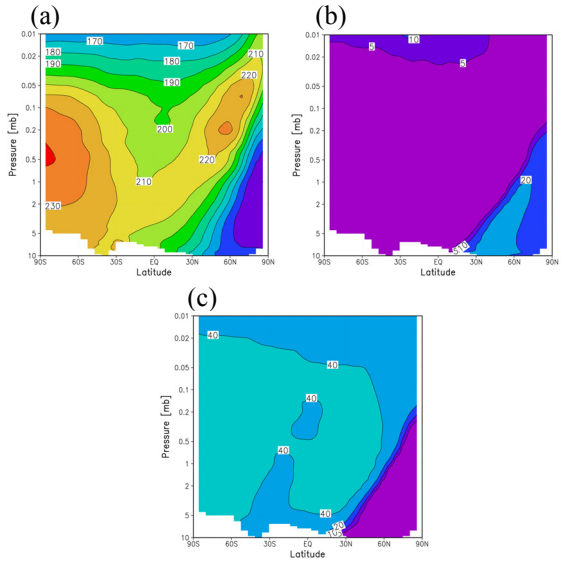

Figure 8: Zonal-mean (a) temperature [K] and mass mixing ratios of (b) water ice and (c) water vapor [ppm] in the global dust storm case in northern winter (*L*s=290˚, visible dust opacity of 4.2).

Future plans: At first, we need to improve the model to obtain the consistent seasonal change of water vapor/ice column density with the MGS-TES observations. In addition, we are going to include the radiative effects of water vapor/ice, HDO cycle, and microphysics among dust, water and CO_2 ice particles.

References: [1] Smith M. D. (2004) *Icarus, 167*, 148-165. [2] Fouchet T. et al. (2007) *Icarus, 190*, 32-49. [3] Encrenaz T. et al. (1991) *Ann. Geophysicae, 9*, 797-803. [4] Encrenaz T. et al. (1995) *Icarus, 113*, 110-118. [5] Clancy R. T. et al. (1996) *Icarus, 122*, 36-62. [6] Kuroda T. et al. (2005) *J. Meteorol. Soc. Japan, 83*, 1-19. [7] Wilson R. J. et al. (2008) *GRL, 35,* doi:10.1029/2007GL032405. [8] Jaquin F. et al. (1986) *Icarus, 68*, 442-461.